processes

MDPI

Article

The Influence of a Manifold Structure on the Measurement Results of a PIV Flowmeter

Huiyu Chen [1,2], Yilong Qiu [1,2,*], Hui Wang [1,2] and Mengjie Gao [3]

[1] Natural Gas Research Institute, PetroChina Southwest Oil & Gas Field Company, Chengdu 610213, China; chhy@petrochina.com.cn (H.C.); wang_hui@petrochina.com.cn (H.W.)
[2] Key Laboratory of Natural Gas Quality Control and Energy Measurement for State Market Regulation, Chengdu 610213, China
[3] China Petroleum Engineering & Construction Corp. Southwest Company, Chengdu 610041, China; gaomengjie_sw@cnpc.com.cn
* Correspondence: qiuyilong@petrochina.com.cn

Abstract: The application of particle image velocimetry (PIV) technology for monitoring natural gas flow is a new method of flow measurement. Since the principle of this technology was proposed, there are still some potential issues. This article investigates the influence of a manifold structure on the measurement results of a PIV flowmeter. A comparison is performed between concentric and eccentric manifold structures, using a circular straight pipe as reference, in terms of the measurement error of the PIV flowmeter and the internal flow state of the natural gas. The results demonstrate that the manifold structure significantly affects the measurement reliability of the PIV flowmeter, especially the eccentric manifold structure. Under flow conditions ranging from 100 to 600 m^3/h, the maximum measurement errors caused by the concentric and eccentric manifold structures are 2.49% and 3.05%, respectively, which show a noticeable increase compared to the maximum measurement error of 2.08% observed for the circular straight pipe. Additionally, the influence of the manifold structure on the downstream flow field is also evident, as the eccentric manifold structure increases the turbulence intensity of the downstream fluid by nearly twofold. The addition of a rectifier can effectively improve the flow state and enhance the measurement reliability of the PIV flowmeter. For the concentric manifold structure under the condition of a 600 m^3/h flow rate, the inclusion of a rectifier produces highly accurate measurement results, similar to those obtained by an ultrasonic flowmeter, with an error value close to zero. This study provides technical support for further promoting the practical application of PIV flowmeters.

Keywords: PIV; natural gas; flow measurement; flow analysis

Citation: Chen, H.; Qiu, Y.; Wang, H.; Gao, M. The Influence of a Manifold Structure on the Measurement Results of a PIV Flowmeter. *Processes* **2024**, *12*, 144. https://doi.org/10.3390/pr12010144

Academic Editors: Jordi de la Hoz, Helena Martin, Ireneusz Zbicinski and Pere Palacín

Received: 8 November 2023
Revised: 4 December 2023
Accepted: 11 December 2023
Published: 7 January 2024

1. Introduction

Natural gas, as a relatively clean fuel, has methane (CH_4) as its main component. During complete combustion, methane reacts with oxygen to produce carbon dioxide (CO_2) and water vapor (H_2O). Since methane molecules contain fewer carbon atoms compared to coal and petroleum, the amount of carbon dioxide emitted from the combustion of an equal mass of natural gas is relatively low [1–3]. With the introduction of the 2030 carbon peak target and the 2060 carbon neutrality vision, reducing greenhouse gas emissions has become a goal pursued by various industries while ensuring efficient industrial development [4–6]. As a result, countries worldwide have observed a sharp increase in the transportation, trading, and use of natural gas.

In the transportation and trading of natural gas, the accuracy of flowmeters is crucial due to the large quantities involved. Currently, ultrasonic flowmeters are being used more frequently in the natural gas trading sector. However, their poor resistance to interference has become an industrial challenge [7]. In previous research, we proposed a particle image velocimetry (PIV) flowmeter [8]. This flowmeter consists of PIV equipment, a

supporting system, and visualized natural gas pipelines. It measures the planar flow field in the pipelines, integrates the circulation, and calculates the flow flux in the natural gas pipelines. The visualization capability, strong anti-interference ability, and non-intrusive measurement method of PIV flow meters are particularly attractive in the industrial field. They eliminate the need for pipeline disassembly during maintenance or replacement. Furthermore, they are not affected by internal impurities within the pipeline. Compared to traditional flow meters, PIV flow meters present significant advantages in terms of installation, maintenance, and other aspects. Experimental measurements show that the measurement deviation of the PIV flowmeter compared to ultrasonic flowmeters is within 2%, confirming its feasibility. As PIV captures tracer particles inside the flow field [9,10], the distribution and tracking characteristics of these particles play a key role in determining the measurement reliability of the PIV flowmeter. Qiu [11] compared the influence of different methods (single pipe, multiple pipes, and an L-shaped pipe) for introducing tracer particles on particle distribution within the pipeline. They found that adding tracer particles to single and multiple pipes had a significant influence on the internal flow field, while the impact of adding particles to the L-shaped pipe was relatively small. However, the particle distribution in the L-shaped pipe was non-uniform. To optimize this, they proposed further improvements, which yielded significant results. Jia Xiaolin [12] conducted research on selecting visualization pipeline materials and found that organic glass had good pressure resistance, transparency, and processability properties, satisfying the requirements of the PIV flowmeter. Ni [13] studied the influence of flow obstacles on the reliability of the PIV flowmeter. The results showed that the relative measurement error of the PIV system flow remained at approximately 1.5% when flow obstacles were installed upstream, and within 0.5% under the baseline state.

The PIV flow meter captures tracer particles on an axially illuminated light sheet formed by a pulsed laser and a beam-steering lens using a CCD camera. The particle velocities are then calculated using cross-correlation algorithms to estimate the fluid velocity, allowing for the determination of cross-sectional flow rates. Through multiple experiments and actual flow rate measurements conducted at the Gas Research Institute of Southwest Oil and Gas Fields Company, we discovered that the complex structural nature of natural gas pipeline networks intensified fluid flow fluctuations in the flow field. This may result in the radial movements of fluid molecules or tracer particles, which makes it difficult for the CCD camera to accurately capture the particle's motion. As a consequence, measurement errors may occur. To further improve the measurement reliability of the PIV flowmeter and identify the physical factors affecting its measurement results, this study conducted flow rate measurements using the PIV flowmeter in downstream areas with different structures, such as single straight pipes (ideal structure), relative manifolds, and misplaced manifolds. The flow characteristics in downstream areas with different manifold structures were studied using visualization methods to analyze the reasons for measurement deviations in the results of the PIV flowmeter. This research provides technical references for the further development of the PIV flowmeter.

2. Materials and Methods

The PIV measurement system used in this study included a pulsed laser, synchronizer (610034, TSI, Shoreview, MN, USA), CCD camera, lens set of a film light source (610021-SOL), and image acquisition and analysis system (TSI Insight 3.0). The overall working mode of the system was a cross-correlation and the maximum measured speed was 500 m/s. The maximum measurement area was 400 mm $\times$ 600 mm, the maximum resolution was 1 mm $\times$ 1 mm, and the maximum frame rate was 15 Hz. The basic parameters of the pulsed laser and CCD camera are shown in Table 1.

Table 1. Basic parameters of pulsed laser and CCD camera.

Pulsed Laser		**CCD Camera**	
Model number	YAG120-NWL	Model number	10–30
Laser power	120 mJ/Pulse	Resolution	1 K × 1 K
Laser pulse frequency	15 Hz	Frame rate	30 frames per second
Input power	2 kW	Lens interface mode	Standard Nikkon port (F Mount)
Pulse duration	3–5 ns	Control mode	Free, cross-frame, single-frame mode
Beam diameter	3.5 mm	Digit	12-bit grayscale image data
Angle of divergence	0.5 mrad	Minimum cross-frame time	Less than 200 to 400 ns
Working mode	Self-triggered, externally triggered	Exportation	12-bit digital output

This study focused on DN100 pipelines and conducted experiments on a 2 MPa pressure pipeline. Due to the flammable and explosive nature of natural gas, there might be safety concerns when pulsing lasers from the PIV system pass through polymethyl methacrylate (organic glass) and irradiate the natural gas. These safety issues include the melting of organic glass or gas explosions. For safety considerations, a systematic analysis of the experiment's safety was performed before testing. We evaluated the energy performance of PIV lasers using transparent plastic sheets and acrylic glass as test materials.

Firstly, the PIV system's pulsed laser (without adding beam splitters; pulsed laser power of 2 W) was directed at a plastic film (as shown in Figure 1). During the 10 min irradiation stage, no significant temperature increase was observed in the plastic film. Then, the plexiglass transparent pipe filled with natural gas (2 MPa) was irradiated from the outside with the same laser intensity and irradiation time, no obvious temperature rise was observed within 10 min, and no melting of the organic glass occurred (as shown in Figure 2), confirming the safety of the experiment.

Figure 1. Irradiation experiment on plastic film.

The working principle of PIV is shown in Figure 3. It utilized the retro-reflective characteristics of tracer particles that were pre-added to the fluid. These particles were captured using a CCD camera, and their motion characteristics within the interrogation area during the time interval between image frames were calculated using cross-correlation algorithms. The average particle motion characteristics within the interrogation area were used to represent the velocity of the fluid in that region. Within the capturing area, multiple sets of interrogation area velocities collectively formed the velocity field of the area, thereby visualizing the fluid velocity.

Figure 2. Irradiation experiment on compressed acrylic pipe.

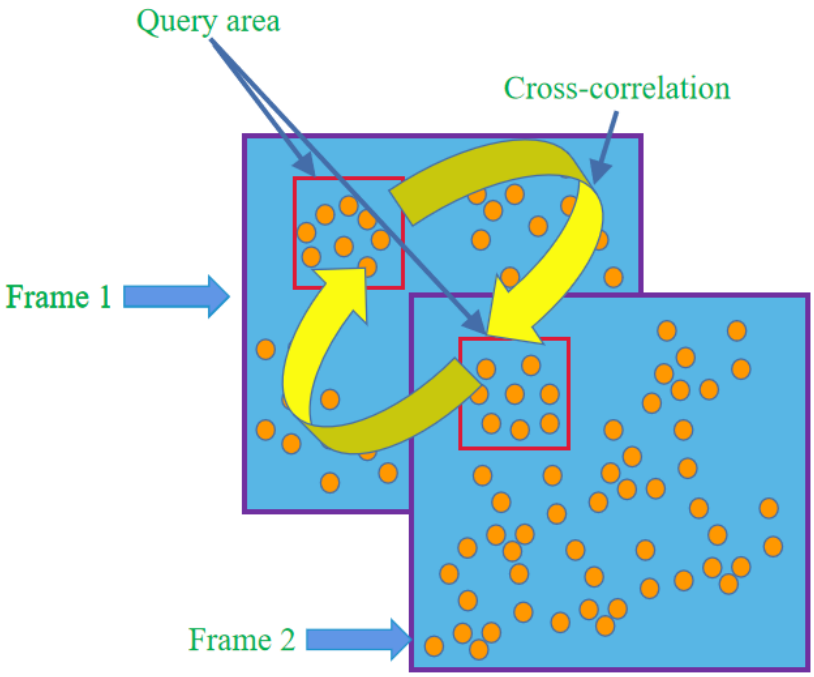

Figure 3. PIV measurement principle [8].

Figure 4 depicts the experimental setup. The focus of this experiment was to investigate the effect of manifold structures on the measurement results of the PIV flowmeter. A straight pipe (ideal state) served as the control group, while the relative manifold and misplaced manifold structures acted as the experimental groups. The downstream flow fields of the manifold structures were measured. Tracer particles added by a particle generator were pressurized using a nitrogen bottle. A four-sided array nozzle structure was used to introduce particles into the main flow field [11]. A PIV flow measurement was performed at a location 16 times larger than the pipe diameter downstream from the nozzle structure. An ultrasonic flowmeter was placed downstream from the PIV measurement area to provide a flow standard. A filter was used to remove tracer particles, allowing clean natural gas to flow downstream.

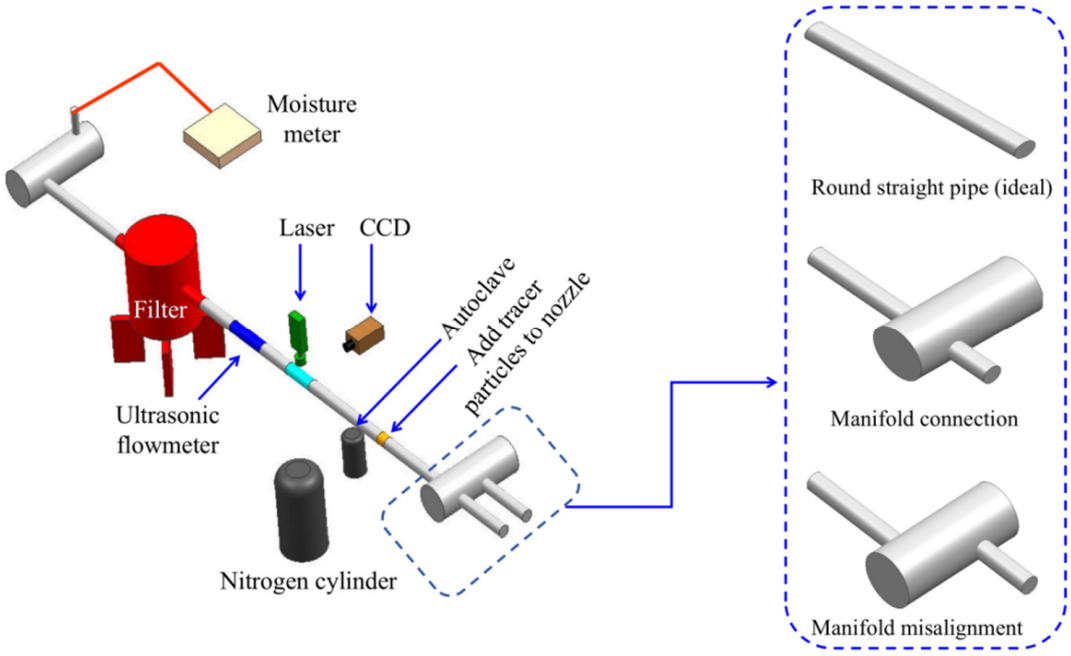

Figure 4. Experimental schematic diagram.

Before starting the experiment, the PIV test system underwent calibrated, which involved the following steps:

(1) Positioning the PIV test system to ensure that the CCD camera and the laser sheet source were perpendicular to each other. Adjusting the distance between the CCD camera and the laser sheet source, ensuring that the imaging area of the CCD camera included the desired test region. Adjusting the focal length of the CCD camera for clear imaging.
(2) Adjusting the time interval between double exposures (Δt) to ensure that more than 3/4 of the tracer particles did not overflow the interrogation area within Δt.
(3) Adjusting the pulse laser energy to achieve clear imaging for both double-exposure images, with the brightness of the two images being roughly equal.
(4) Fine-tuning the addition of tracer particles to ensure a uniform distribution within the test area and moderate concentration. This ensured that there were enough tracer particles in the test area without creating overexposure in the CCD camera.

Through continuous on-site calibrations, the entire system met the testing requirements.

Three installation conditions (ideal state, relative manifold, and misplaced manifold) and six different flow rates (100 m^3/h, 200 m^3/h, ^{3}00 m^3/h, 400 m^3/h, 500 m^3/h, and 600 m^3/h) were selected for PIV testing. For each operating condition, the PIV system was applied for testing. Once the system reached stability under each condition, 6 sets of raw images of the flow field inside the pipe were captured (acquired at a frequency of 15 Hz). Then, analysis software provided with the PIV system (Insight and Tecplot) was used to analyze the images and obtain relevant flow field information.

Figure 5 is a live photo taken at the Natural Gas Research Institute of China Petroleum Southwest Oil and Gas Field Company (Chengdu, China). The transparent pipeline used for the experiment was connected to the DN100 natural gas transport pipeline through a flange. Before the experiment, the pipeline was tested for leaks, and no leakage was found, ensuring a safe environment for the experiment. The entire transportation pipeline and the inlet pipe diameter were both 100 mm, while the mixing manifold structure pipe diameter was 300 mm.

Figure 5. Experimental site diagram.

3. Theoretical Analysis

When conducting high-pressure natural gas transportation in the DN100 pipeline, the internal flow conformed to the assumption of a source-free flow field and followed the mass conservation equation, as shown in Equation (1) [14,15]. The influence of external forces, such as resistance from flow components and viscous drag on the flow field characteristics during the internal flow process, complied with the Navier–Stokes equations, as shown in Equation (2) [16,17]:

$$\frac{\partial \rho}{\partial t} + \nabla \cdot (\rho \boldsymbol{v}) = 0 \tag{1}$$

$$\frac{\partial (\rho \boldsymbol{v})}{\partial t} + \nabla \cdot (\rho \boldsymbol{v}\boldsymbol{v}) = -\nabla p + \mu \nabla^2 \boldsymbol{v} + \boldsymbol{f} \tag{2}$$

In the equation, ρ represents the fluid density, kg/m^3; t represents the time, s; $\boldsymbol{v}$ is the fluid velocity, m/s; p denotes the fluid pressure, Pa; μ is the fluid viscosity, Pa·s; and $\boldsymbol{f}$ represents the external force acting on the unit volume of fluid, N/m^3.

We evaluated the stability of the flow field based on the level of fluctuation using the concept of turbulence intensity, which quantitatively described the fluctuation characteristics of the flow field. Its basic definition is given by Equation (3) [18–20]:

$$I = \frac{v'}{\overline{v}} = 0.16\,(Re)^{-\frac{1}{8}} \tag{3}$$

In the equation, I represents the turbulence intensity; v' denotes the velocity fluctuations in the flow field, m/s; $\overline{v}$ represents the mean velocity in the flow field, m/s; and Re is the Reynolds number of the flow field.

The principle of PIV (particle image velocimetry) flow metering involves dividing the circular cross-section of a DN100 pipe into evenly spaced concentric rings. The measured particle velocities represent the velocity at each ring's surface. Finally, by summing the products of the ring areas and corresponding velocities, the total flow rate across the entire cross-section was obtained. The integration formula is given by Equation (4). For specific integration methods, please refer to our previously published paper [8].

$$Q = \frac{\sum_1^n V_n}{n} S \tag{4}$$

In the equation, Q represents the flow rate through the cross-section of the pipe, m^3/s; n denotes the number of query regions; V_n represents the velocity in each query region, m/s; and S represents the cross-sectional area of the pipe, m^2.

4. Result Analysis

4.1. Influence of Manifold Structure on the Measurement Results

Figure 6 presents the data obtained from the experiments conducted at the Natural Gas Research Institute of Southwest Oil and Gas Field Corporation in China. Due to the manual control of the on-site flow regulation equipment using valves, it was not possible to accurately adjust the flow rate to a regular pattern. Therefore, only an approximate representation of six flow rate conditions could be achieved. From Figure 6A, it can

be observed that, under ideal conditions, when the flow rate is less than 300 m^3/h, the measurement results of the PIV and ultrasonic flowmeters are almost the same. However, as the flow rate exceeds 300 m^3/h, the PIV flowmeter measurements are lower than those of the ultrasonic flowmeter, and the deviation increases with the increasing flow rate. This phenomenon occurs because, under high flow rate conditions, the flow inside the pipeline becomes unstable, resulting in greater deviations due to the higher flow rates. However, by comparing the relative errors, it can be observed that the relative error for high flow rate conditions is significantly lower than that for low flow rate conditions. Among the six flow rate conditions tested, the highest relative error occurred at a flow rate of 600 m^3/h, with an error value of 2.08%, indicating the reliability of the experimental method.

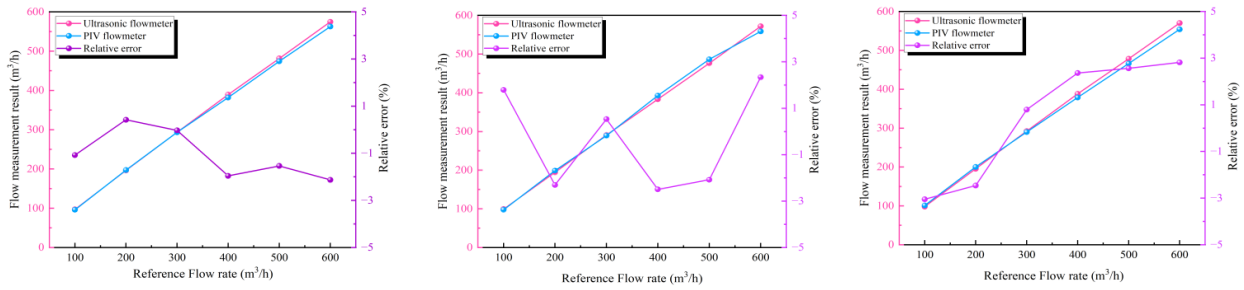

Figure 6. Flow measurement results under ideal conditions ((**A**): ideal condition; (**B**): manifold relative; (**C**): manifold misalignment).

Figure 6B presents the measurement results under the manifold structure condition. In the presence of the manifold structure, due to the smaller diameter of the inlet pipe (DN100) compared to the manifold pipe diameter (DN300), when natural gas entered the manifold structure, it initially expanded, causing a disarray of the fluid molecules. Subsequently, as the natural gas flowed from the manifold structure into the main pipeline (DN100), a compression process occurred, further increasing the disorderliness of the fluid and intensifying the turbulence.

These flow patterns resulted in an increased level of fluctuation in the movement of fluid molecules within the PIV measurement section, causing tracer particles to experience longitudinal motion and escape the capture range of the CCD camera. This led to the decreased reliability of the measurements. Therefore, compared to the ideal condition, the measurement error of the PIV flowmeter increased with the presence of a manifold structure. The maximum error occurred at a flow rate of 400 m^3/h, with a value of −2.49%. Despite the slight increase in the relative error, the overall measurement results remained relatively accurate.

Figure 6C shows the measurement results with the presence of a misplaced manifold structure. Compared to the previous two cases, the misplaced manifold structure further increased the complexity of the flow, resulting in an increased flow instability with phenomena such as the expansion, compression, and collision of the gas flow within the manifold structure. This led to an increased level of turbulence in the flow field, consequently increasing the measurement error of the PIV flowmeter, with a maximum relative error exceeding 3.0%. From the comparison of these three cases, it can be concluded that flow instability is a critical factor influencing the measurement reliability of the PIV flowmeter.

Figure 7 illustrates the variations of relative errors (absolute values) for each set of operating conditions.

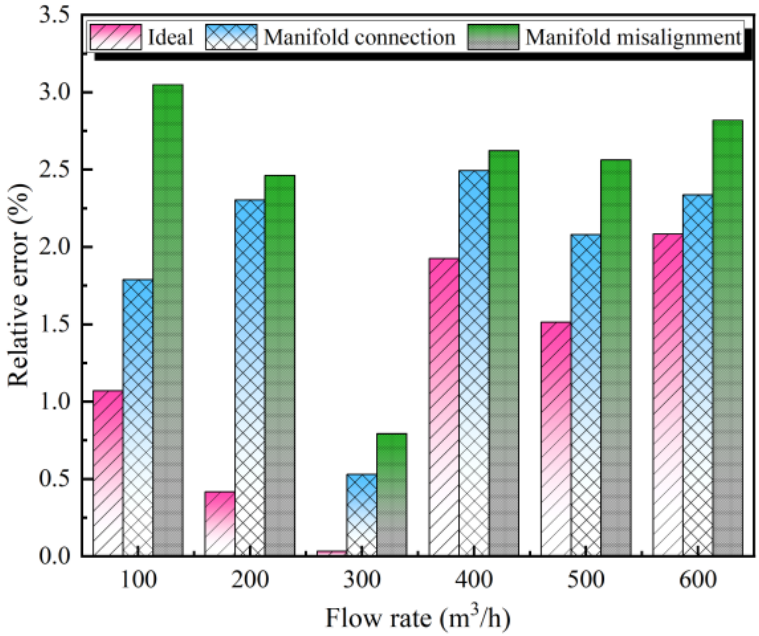

Figure 7. Relative error of measurements under different working conditions.

Figure 7 shows the relative errors of flow metering for different manifold structures. The relative error was calculated as follows: Relative error = 100 × (ultrasonic flowmeter measurement result—PIV flowmeter measurement result)/ultrasonic flowmeter measurement result. It can be clearly observed that, under different flow rates, the maximum measurement error occurs with the misplaced manifold structure. In ideal, manifold-relative, and misplaced manifold conditions, the minimum relative error was observed at a flow rate of 300 m^3/h. When deviating from this condition (increasing or decreasing the flow rate), the relative error increased significantly. At low flow rates, the flow inside the pipeline was not fully developed [21–25], resulting in flow field fluctuations and greater measurement errors. As the flow rate increased, the flow became more developed, and the irregular flow field tended to become more regular, which reduced the measurement error. However, when the flow rate exceeded 300 m^3/h, the flow experienced strong collisions with various flow obstacles inside the pipeline, leading to significant flow field fluctuations and an increase in the measurement error once again.

4.2. Influence of the Manifold Structure on Flow Field Turbulence Intensity

To further analyze the turbulence characteristics induced by the manifold structure in the downstream flow field, the turbulence intensity in the central region of the PIV measurement area was monitored. Due to the axisymmetric nature of the circular pipe, only the measurement line along one radius direction on the cross-section was studied. The positions of the measurement lines are shown in Figure 8.

Figure 9 shows the distribution curves of the turbulence intensity under different operating conditions. As shown in Figure 9A, under ideal conditions, the distribution pattern of the turbulence intensity is similar for different flow rates. It gradually increases from the wall towards the center of the pipe, and the curve is relatively smooth. Due to the constraints of the wall and the influence of the fluid boundary layer, the fluid fluctuation near the wall is generally low. Therefore, the flow near the wall is more stable. Within a distance of 30 mm from the wall, the turbulence intensity ranges between 2% and 5% (this pattern applies to all flow rate conditions). As the distance from the wall increases, the restraining effect of the wall on the fluid decreases, and fluid pulsations become evident, resulting in an increase in the turbulence intensity. The maximum turbulence intensity occurs at the pipe center and ranges between 6% and 7.5%.

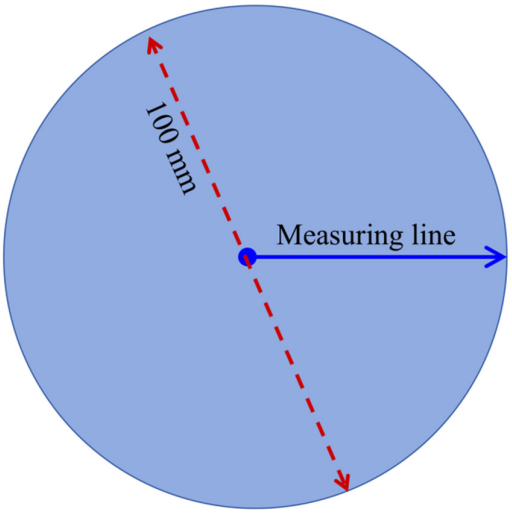

Figure 8. Schematic diagram of measurement line.

Figure 9B shows the turbulence intensity distribution curve under the relative structure of the collecting tube. Compared to the ideal condition, the turbulence distribution in this structure becomes more chaotic. Particularly at flow rates of 400 and 600 m^3/h, the turbulence intensity curve exhibits fluctuations, indicating flow instability. However, the overall pattern of increasing turbulence intensity from the wall along the radius remains consistent. In this condition, the maximum turbulence intensity occurs at the flow rate of 600 m^3/h, with a value of 13.11%, which is close to twice the maximum turbulence intensity observed in the ideal condition.

Figure 9C represents the turbulence intensity distribution curve under the staggered structure of the collecting tube. In the complex piping structure, the fluid trajectories become even more chaotic, making the regularity in the distribution curve less obvious, with multiple peak values observed. The maximum turbulence intensity occurs at the 600 m^3/h condition, with a value of 14.32%. The fluctuation characteristics of the flow field intensify, making this flow field unfavorable for PIV flowmeter measurements.

Under all operating conditions, the turbulence intensity value was relatively low at a flow rate of 300 m^3/h. Increasing or decreasing the flow rate enhances the turbulence intensity inside the pipe, which is consistent with the findings in Section 4.1, further verifying that flow instability can affect the measurement reliability of PIV flowmeters.

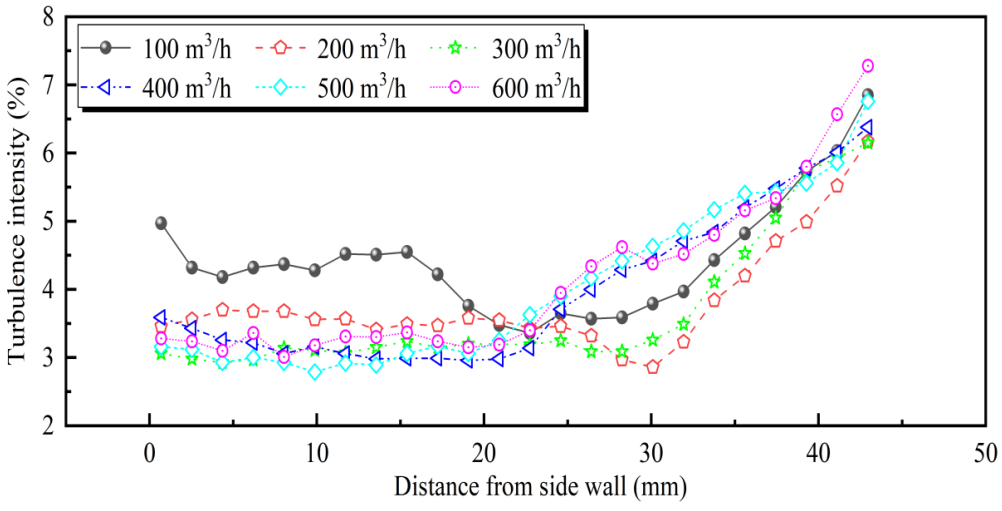

(A)

Figure 9. *Cont.*

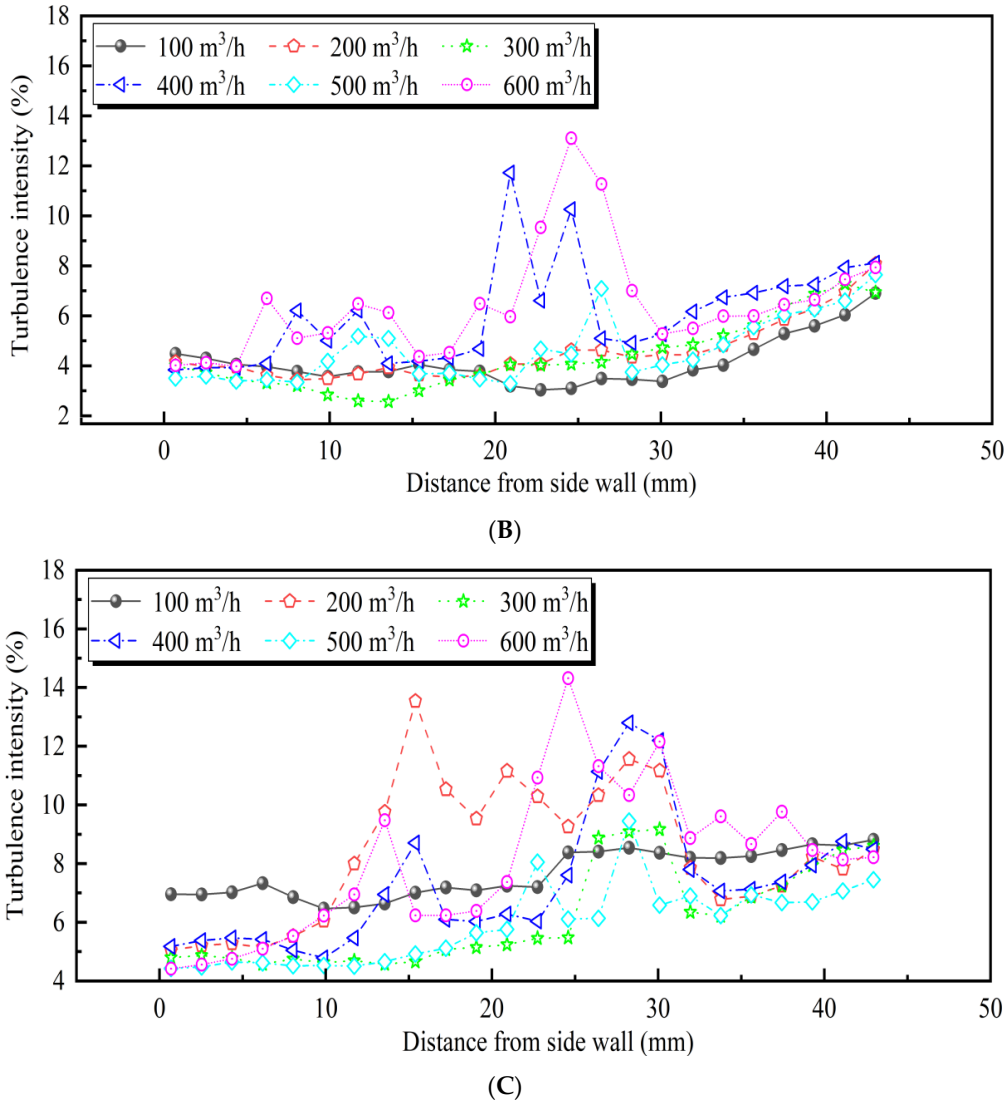

Figure 9. Distribution of turbulence intensity inside the pipeline ((**A**): ideal condition; (**B**): manifold relative; (**C**): manifold misalignment).

4.3. The Inhibitory Effect of Rectifiers on Unstable Flow Fields

Based on the analyses presented in Sections 4.1 and 4.2, the impact of collector structures on the measurement results of PIV flowmeters mainly lies in inducing flow field instability. Therefore, adding rectifier devices between the collector structure and the PIV flowmeter can stabilize the flow field and improve the measurement reliability and applicability of PIV flowmeters.

Figure 10 shows the measurement results of the turbulence intensities for different collector structures with the addition of rectifier devices. It can be observed from Figure 10 that the effect of rectifiers on reducing the turbulence intensity is not significant when the flow rate is below 300 m^3/h. The main cause of flow instability is insufficient flow development, and adding rectifiers primarily reduces the occurrence of flow field fluctuations. Therefore, the effect of rectifiers is not obvious at low flow rates, and in some cases, it may even increase the turbulence intensity due to the added complexity of the internal structure caused by the rectifiers, for example, at a distance of 20–30 mm from the pipe wall under the 100 m^3/h condition and 10–20 mm under the 200 m^3/h condition.

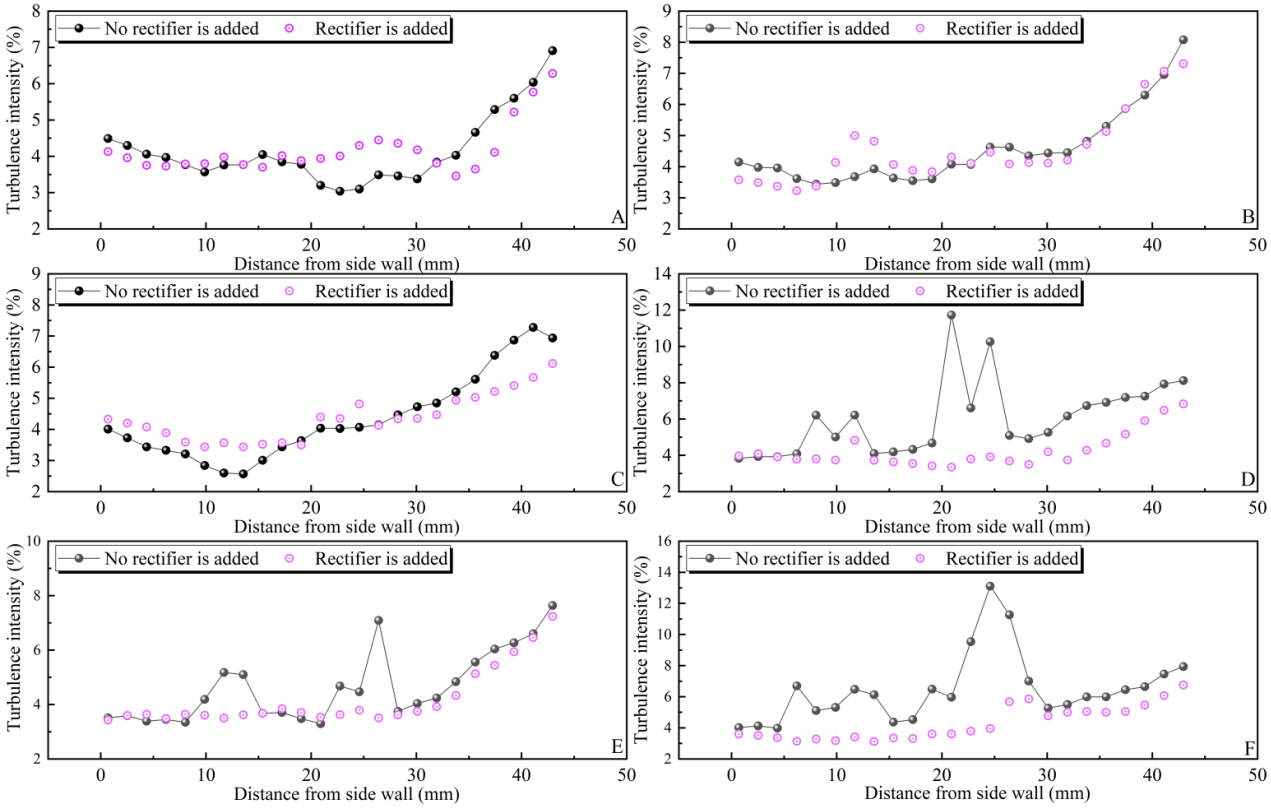

Figure 10. The role of the rectifier in reducing turbulence intensity in the relative structure of the manifold structure.

As the flow rate increases, the main cause of flow disturbance shifts from insufficient development to flow collision. At this stage, the role of rectifiers becomes evident. They make the flow more regular for turbulent fluids. Therefore, in the range of 400–600 m^3/h, the flow field turbulence intensity with rectifiers is significantly lower than without rectifiers. Additionally, the maximum turbulence intensity decreases by 42% and 48% in the 400 and 600 m^3/h flow rate conditions, respectively.

The addition of rectifiers throughout the entire measured flow range of the relative collector structure has a uniformizing effect on the flow field. Although the effect of reducing turbulence intensity values is not significant at low flow rates, the uniform distribution of flow velocity has positive implications for improving the measurement reliability of PIV flowmeters. Therefore, adding rectifiers to the relative collector structure can help improve the measurement reliability of PIV flowmeters.

Figure 11 illustrates the effect of rectifiers on reducing the turbulence intensity in the staggered collector structure. In the staggered collector structure, the turbulence of the fluid was mainly caused by phenomena such as expansion, compression, and collision occurring within the collector structure. This type of flow is characterized by turbulent and disordered movement. Therefore, in the staggered collector structure, the role of rectifiers was evident.

As shown in Figure 11, under various flow rate conditions, the rectifiers significantly reduced the turbulence intensity within the fluid. The reduction demonstrated clear regularity. However, in the 600 m^3/h flow rate condition, the turbulence intensity distribution curve still exhibited some peak values along the radial direction, such as at a distance of 20–30 mm from the pipe wall. In high flow rate conditions, the phenomenon of fluid collision became significant. Although the rectifiers could partially suppress the occurrence of an unstable flow, their effect was limited, leading to some remaining fluctuations. However, overall, the addition of rectifiers greatly improved the flow field distribution in the staggered collector structure.

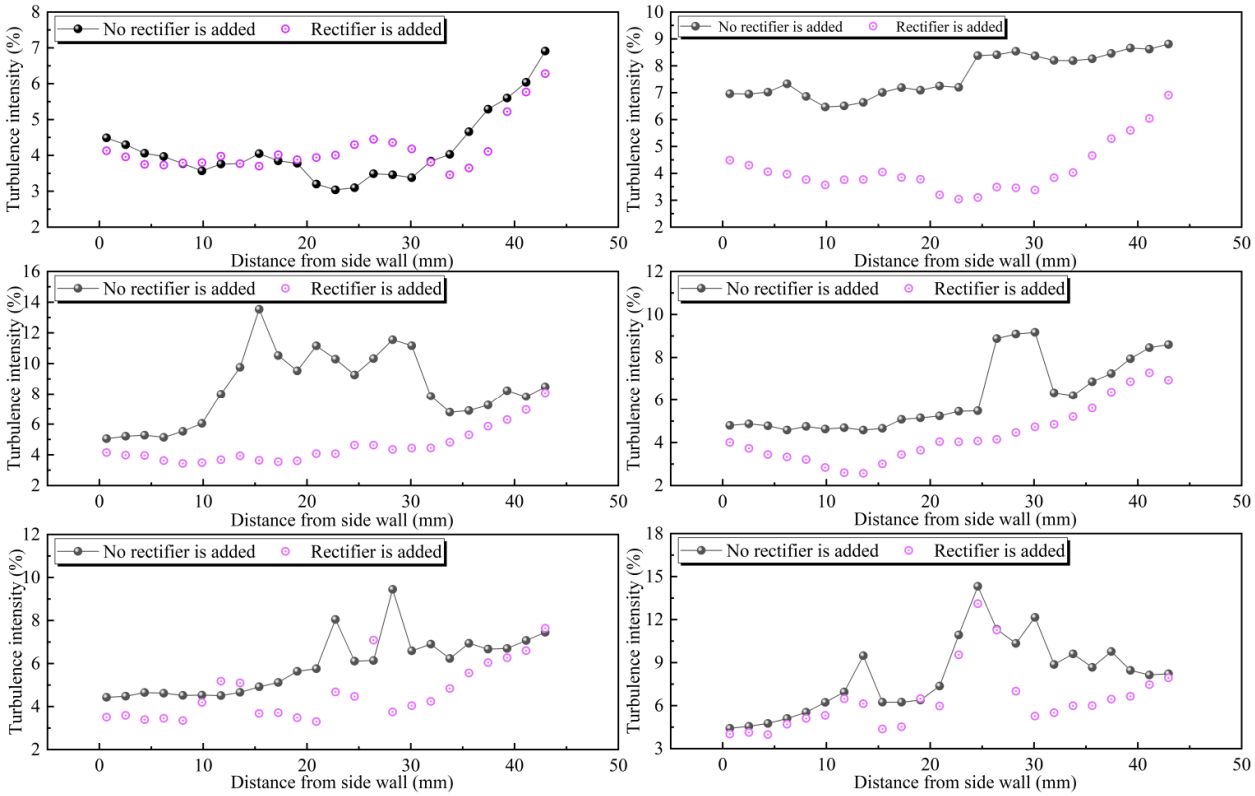

Figure 11. The effect of the rectifier on reducing the turbulence intensity in the manifold-phase disjunction structure.

4.4. The Impact of Rectifiers on the Measurement Results of PIV Flowmeters

Figure 12 demonstrates the measurement errors of PIV flowmeters under different conditions with the addition of rectifiers. As shown in Figure 12, the inclusion of rectifiers significantly reduces the deviation between the measurement results of PIV and ultrasonic flowmeters. For the relative and staggered collector structures, the extent of reduction in the measurement error for each flow rate condition (the decrease in measurement error = 100 × (absolute error without rectifiers − absolute error with rectifiers)/absolute error without rectifiers) is presented in Table 2.

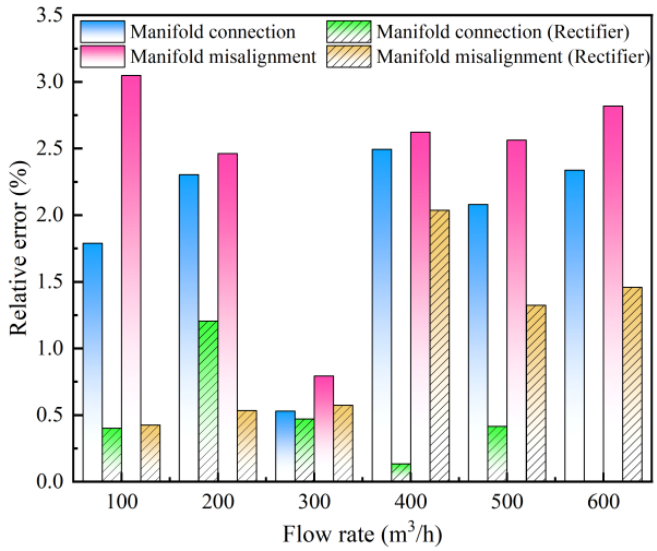

Figure 12. Influence of rectifier on measurement errors of a PIV flowmeter.

Table 2. Measurement results of flowmeter under different working conditions (m^3/h).

Flow Value	Manifold Connection			Manifold Connection (Rectifier)			Measurement Error Reduction Value
	Ultrasonic Flowmeter	PIV Flowmeter	Error	Ultrasonic Flowmeter	PIV Flowmeter	Error	
100	99.49	97.71	1.79%	99.73	99.33	0.40%	77.58%
200	194.39	198.87	2.30%	195.90	193.54	1.20%	47.73%
300	290.54	289.00	0.53%	291.23	289.86	0.47%	11.25%
400	383.23	392.79	2.49%	385.46	385.98	0.13%	94.59%
500	476.37	486.28	2.08%	478.32	476.33	0.41%	80.00%
600	571.73	558.37	2.33%	563.49	563.51	0.00%	99.85%
Flow Value	**Manifold Misalignment**			**Manifold Misalignment (Rectifier)**			**Measurement Error Reduction Value**
	Ultrasonic Flowmeter	**PIV Flowmeter**	**Error**	**Ultrasonic Flowmeter**	**PIV Flowmeter**	**Error**	
100	98.07	101.06	3.05%	98.67	98.25	0.43%	86.04%
200	195.43	200.24	2.46%	196.77	195.72	0.53%	78.32%
300	292.28	289.96	0.79%	291.47	285.24	2.14%	27.63%
400	388.05	378.88	2.36%	384.90	377.06	2.04%	22.35%
500	478.41	466.15	2.56%	475.54	469.24	1.32%	48.30%
600	570.18	554.11	2.82%	564.30	556.07	1.46%	48.25%

Particularly, in the case of the relative collector structure at a 600 m^3/h flow rate, the addition of rectifiers made the measurement results for the PIV flowmeters very close to those of the ultrasonic flowmeters, with the relative error approaching zero. Even in stable flow conditions (300 m^3/h), the inclusion of rectifiers had a positive effect on improving the measurement reliability of the PIV flowmeters.

From this, we can conclude that adding rectifier structures above the collector in the usage of PIV flowmeters for flow measurements results in more accurate measurements.

5. Conclusions

In this paper, the influence of a manifold structure on the measurement results of a PIV flowmeter was studied experimentally, and the fluid flow state in the test area was monitored using a PIV experiment, which further revealed the relationship between the flow state and measurement results of the PIV flowmeter. The rectifier structure was proposed to reduce the flow fluctuation caused by the manifold structure, and the specific conclusions were as follows:

(1) The manifold structure had a significant impact on the measurement results of the PIV flowmeter. When the flow value was between 100 m^3/h and 600 m^3/h and there was no manifold structure, the maximum deviation of the PIV and ultrasonic flowmeters was 2.08%. When there was a manifold structure, the error value significantly increased, and the maximum deviation of the flow measurement results of the manifold-relative and manifold-phase disjunction structures were 2.49% and 3.05%, respectively.

(2) The manifold structure caused the instability of the downstream pipeline flow. The metering results of the PIV flowmeter were affected by the stability of the flow field. When there was a manifold structure present, the flow in the metering section of the PIV flowmeter was unstable due to the bad flow states, such as expansion, compression, and collision. The flow value was between 100 m^3/h and 600 m^3/h. The maximum turbulence intensities created by the manifold-relative and manifold-phase disjunction structures were 13.11% and 14.32%, respectively, which were nearly twice the maximum turbulence intensity value of the structure without a manifold.

(3) The rectifier structure played an active role in improving the reliability of the PIV flowmeter. Adding a rectifier between the manifold structure and the measuring section of the PIV flowmeter could significantly improve the measuring reliability of the PIV

flowmeter and reduce the turbulence intensity of the main pipeline flow field. Under the flow condition of 400,600 m^3/h relative to the manifold structure, the addition of the rectifier reduced the maximum turbulence intensity by 42% and 48%, respectively. In the flow condition of 100–600 m^3/h of the manifold-phase disjunction structure, the effect of the rectifier on reducing the turbulence intensity was very significant. The addition of a rectifier improved the measuring reliability of the PIV flowmeter in the manifold-relative and manifold-phase disjunction structures. Especially in the flow condition of the manifold-relative structure (600 m^3/h), the deviation of the measuring result between the PIV and ultrasonic flowmeters tended to 0.

Author Contributions: Conceptualization, Y.Q. and M.G.; methodology, H.W.; software, H.C.; validation, Y.Q. and H.C. All authors have read and agreed to the published version of the manuscript.

Funding: This research received no external funding.

Data Availability Statement: Data are contained within the article.

Conflicts of Interest: Huiyu Chen, Yilong Qiu and Hui Wang were employed by the Natural Gas Research Institute, PetroChina Southwest Oil & Gas Field Company, Mengjie Gao was employed by the China Petroleum Engineering & Construction Corp. Southwest Company.

References

1. Ríos-Mercado, R.Z.; Borraz-Sánchez, C. Optimization problems in natural gas transportation systems: A state-of-the-art review. *Appl. Energy* **2015**, *147*, 536–555. [CrossRef]
2. Rajnauth, J.; Ayeni, K.; Barrufet, M. Gas transportation: Present and future. In Proceedings of the SPE Unconventional Resources Conference/Gas Technology Symposium, Calgary, AB, Canada, 16–19 June 2008; SPE-114935-MS.
3. Taheri, Z.; Shabani, M.R.; Nazari, K.; Mehdizaheh, A. Natural gas transportation and storage by hydrate technology: Iran case study. *J. Nat. Gas Sci. Eng.* **2014**, *21*, 846–849. [CrossRef]
4. Li, W.; Li, Z.; Qin, Z.; Yan, S.; Wang, Z.; Peng, S. Influence of the solution pH on the design of a hydro-mechanical magneto-hydraulic sealing device. *Eng. Fail. Anal.* **2022**, *135*, 106091. [CrossRef]
5. Li, Z.; Li, W.; Wang, Q.; Xiang, R.; Cheng, J.; Han, W.; Yan, Z. Effects of medium fluid cavitation on fluctuation characteristics of magnetic fluid seal interface in agricultural centrifugal pump. *Int. J. Agric. Biol. Eng.* **2021**, *14*, 85–92. [CrossRef]
6. Yu, H.; Zhao, W.; Ma, F.; Zeng, K.; Ma, F. Assessing the effects of agricultural waste returning on soil moisture characteristics. *Environ. Progress Sustain. Energy* **2023**, e14314. [CrossRef]
7. Yudong, T. Study on Measuring Large Flow of Natural Gas by PIV and LDV. Ph.D. Thesis, Xihua University, Chengdu, China, 2010.
8. Wangxu, L.; Zhenggui, L.; Wanquan, D.; Lei, J.; Yilong, Q.; Huiyu, C. Particle image velocimetry flowmeter for natural gas applications. *Flow Meas. Instrum.* **2021**, *82*, 102072. [CrossRef]
9. Grant, I. Particle image velocimetry: A review. *Proc. Inst. Mechan. Eng. Part C J. Mechan. Eng. Sci.* **1997**, *211*, 55–76. [CrossRef]
10. Adrian, R.J. Twenty years of particle image velocimetry. *Exp. Fluids* **2005**, *39*, 159–169. [CrossRef]
11. Qiu, Y.; Chen, H.; Li, W.; Wu, F.; Li, Z. Optimization of the tracer particle addition method for PIV flowmeters. *Processes* **2021**, *9*, 1614. [CrossRef]
12. Xiaolin, J.; Yubo, C.; Xun, L. Research on key technologies of natural gas pipeline internal flow field test system. *Ind. Metrol.* **2015**, *25*, 5–9.
13. Rui, N.; ShuYan, Y.; Daibing, Z. Application of particle imaging velocity measurement technology in natural gas measurement. *Nat. Gas Oil* **2014**, *32*, 77–80+1–2.
14. Li, W.; Li, Z.; Han, W.; Li, Y.; Yan, S.; Zhao, Q.; Gu, Z. Pumping-velocity variation mechanisms of a ferrofluid micropump and structural optimization for reflow inhibition. *Phys. Fluids* **2023**, *35*, 052005.
15. Li, W.; Li, Z.; Han, W.; Li, Y.; Yan, S.; Zhao, Q.; Chen, F. Measured viscosity characteristics of Fe_3O_4 ferrofluid in magnetic and thermal fields. *Phys. Fluids* **2023**, *35*, 012002. [CrossRef]
16. Kan, K.; Binama, M.; Chen, H.; Zheng, Y.; Zhou, D.; Su, W.; Muhirwa, A. Pump as turbine cavitation performance for both conventional and reverse operating modes: A review. *Renew. Sustain. Energy Rev.* **2022**, *168*, 112786. [CrossRef]
17. Kan, K.; Xu, Y.; Li, Z.; Xu, H.; Chen, H.; Zi, D.; Gao, Q.; Shen, L. Numerical study of instability mechanism in the air-core vortex formation process. *Eng. Appl. Comput. Fluid Mech.* **2023**, *17*, 2156926. [CrossRef]
18. Li, W.; Li, Z.; Wang, Z.; Wu, F.; Xu, L.; Peng, S. Turbulence intensity characteristics of a magnetoliquid seal interface in a liquid environment. *Coatings* **2021**, *11*, 1333. [CrossRef]
19. Gaurier, B.; Carlier, C.; Germain, G.; Pinon, G.; Rivoalen, E. Three tidal turbines in interaction: An experimental study of turbulence intensity effects on wakes and turbine performance. *Renew. Energy* **2020**, *148*, 1150–1164. [CrossRef]
20. Arenas-López, J.P.; Badaoui, M. Stochastic modelling of wind speeds based on turbulence intensity. *Renew. Energy* **2020**, *155*, 10–22. [CrossRef]

21. Zhang, Y.; Zang, W.; Zheng, J.; Cappietti, L.; Zhang, J.; Zheng, Y.; Fernandez-Rodriguez, E. The Influence of Waves Propagating with the Current on the Wake of a Tidal Stream Turbine. *Appl. Energy* **2021**, *290*, 116729. [CrossRef]
22. Xu, J.; Zhang, Y.; Peng, B.; Zheng, Y.; Li, C.; Zang, W.; Fernandez-Rodriguez, E. Study on the Dynamics and Wake Characteristics of a Floating Tidal Stream Turbine with Pitch Motion under Free Surface. *Phys. Fluids* **2023**, *35*, 085101. [CrossRef]
23. Ren, Z.; Li, D.; Fu, X.; Wang, H.; Liu, J.; Li, Y. Synergistic effects of vapor and gaseous cavitation and mass-transfer mechanism in a mechanical pump. *Phys. Fluids* **2023**, *35*, 053335.
24. Ren, Z.; Li, D.; Wang, C.; Wang, H.; Liu, J.; Li, Y. Hump and mass-transfer characteristics of dissolved oxygen induced by gaseous cavitation in a space micropump. *Int. Commun. Heat Mass Transf.* **2023**, *145*, 106830. [CrossRef]
25. U.S. Energy Information Administration. *Natural Gas Processing: The Crucial Link between Natural Gas Production and Its Transportation to Market*; U.S. Energy Information Administration: Los Alamos, NM, USA, 2006; pp. 20–22.